ChemPubSoc Europe

DOI: 10.1002/chem.201601499

CHEMISTRY A European Journal Full Paper

Fluorescent Probes

Rational Design of Fluorescent Phthalazinone Derivatives for One- and Two-Photon Imaging

Lingfei Yang[+],[a, c] Yuanjun Zhu[+],[b] Mengyang Shui,[b] Tongliang Zhou,[a] Yuanbo Cai,[d] Wei Wang,[a] Fengrong Xu,[a] Yan Niu,[a] Chao Wang,[a] Jun-Long Zhang,[d] Ping Xu,*[a] Lan Yuan,*[c] and Lei Liang*[a]

Abstract: Phthalazinone derivatives were designed as optical probes for one- and two-photon fluorescence microscopy imaging. The design strategy involves stepwise extension and modification of pyridazinone by 1) expansion of pyridazinone to phthalazinone, a larger conjugated system, as the electron acceptor, 2) coupling of electron-donating aromatic groups such as *N*,*N*-diethylaminophenyl, thienyl, naphthyl, and quinolyl to the phthalazinone, and 3) anchoring of an alkyl chain to the phthalazinone with various terminal substituents such as triphenylphosphonio, morpholino, triethylammonio, *N*-methylimidazolio, pyrrolidino, and piperidino. Theoretical calculations were utilized to verify the initial design. The desired fluorescent probes were synthesized by two different routes in considerable yields. Twenty-two phthalazinone derivatives were synthesized and their photophysical properties were measured. Selected compounds were applied in cell imaging, and valuable information was obtained. Furthermore, the designed compounds showed excellent performance in two-photon microscopic imaging of mouse brain slices.

Introduction

Fluorescence imaging for observing life processes in single molecules, living cells, and deep tissues attracts attention in fundamental medicine, clinical diagnostics, and drug discovery.[1] As chemobiological tools, fluorescent probes have been developed with extraordinary luminescence, accurate localization, excellent spatial resolution, and high sensitivity through continuous efforts to improve their structures and related properties.[2] Apart from optimization of the basic optical properties, improved applicability with the aim of visualizing specific subcellular organelles and large-scale tissues is a critical issue. Hence, the development of suitable fluorescent probes to decipher local information on intracellular and extensive regions of tissues is required.[3]

On the subcellular level, there has been broad interest in developing novel imaging techniques and dyes for cellular organization, structures, and molecular events during biological processes. Many existing fluorophores, such as fluorescein, rhodamine, coumarin, cyanine, and BODIPY, have exhibited good applicability and promising prospects.[4] Furthermore, to improve the physical and chemical properties and enhance the performance, the development of novel fluorescent probes with appropriate solubility, high luminescence, low toxicity, high stability, and large Stokes shift is still required. Besides, efficient synthesis and easy modification are also in demand for building large libraries of compounds.

Both one-photon microscopy (OPM) and two-photon microscopy (TPM), which utilizes two near-infrared (NIR) photons as the excitation light source, have emerged as powerful imaging tools for biological and medicinal research. These two techniques have their own advantages and limitations, and thus they are often utilized complementarily depending on the specific application.[5] For example, OPM is capable of imaging fixed thin samples with high resolution, especially for cell imaging, and TPM offers advantages such as longer observation duration, deep penetration into tissues, and low phototoxicity. Therefore, a variety of two-photon probes have been developed, and their utility in bioimaging applications has been demonstrated.[6] To meet the requirements of both OPM and TPM imaging techniques, herein we designed a novel type of fluorescent probes by rational design and theoretical calculations.

[a] L. Yang,[+] T. Zhou, W. Wang, F. Xu, Y. Niu, C. Wang, Prof. Dr. P. Xu, Prof. Dr. L. Liang
Department of Medicinal Chemistry, School of Pharmaceutical Sciences
Peking University Health Science Center, Beijing (P. R. China)
E-mail: pingxu@bjmu.edu.cn
leiliang@bjmu.edu.cn

[b] Dr. Y. Zhu,[+] M. Shui
Department of Molecular and Cellular Pharmacology
School of Pharmaceutical Sciences, Peking University, Beijing (P. R. China)

[c] L. Yang,[+] Dr. L. Yuan
Medical and Healthy Analysis Center, Peking University, Beijing (P. R. China)
E-mail: yuan_lan@bjmu.edu.cn

[d] Y. Cai, Prof. Dr. J.-L. Zhang
Beijing National Laboratory for Molecular Science
State Key Laboratory of Rare Earth Materials Chemistry and Applications
College of Chemistry and Molecular Engineering
Peking University, Beijing (P. R.China)

[+] These authors contributed equally to this work.

Supporting information for this article, including all experimental details, can be found under http://dx.doi.org/10.1002/chem.201401499.

Pyridazinone, a six-membered aromatic ring which is not naturally synthesized in living organisms, has been synthetically prepared and applied as a pharmacophore in drug design.[7] Pyridazinones have been developed as phosphodiesterase III inhibitors, α1-adrenoreceptor antagonists, antiplatelet agents, anti-inflammatory agents, HIV-1 reverse-transcriptase inhibitors, GPCR antagonists, and c-Met inhibitors.[8] Previously, we designed a series of full-color tunable fluorescent dyes based on a pyridazinone scaffold. Preliminary application of these pyridazinone derivatives in cell imaging revealed ideal cell permeability and high stability.[9] To meet the requirements of biological research, we have now employed phthalazinone, an analogue of pyridazinone, to construct a novel fluorophore. To the best of our knowledge, phthalazinone has never been used in the development of fluorescent probes.

Results and Discussion

Design and computational verification

To fulfil our aim of utilizing phthalazin-1(2*H*)-one, we chose 6-phenylpyridazinone as the initial electron-withdrawing moiety to build the fluorescent core skeleton. Conjugation with a benzene ring at the 4,5-positions of pyridazinone yields phthalazinone with a larger π-system as electron acceptor (Figure 1 a).

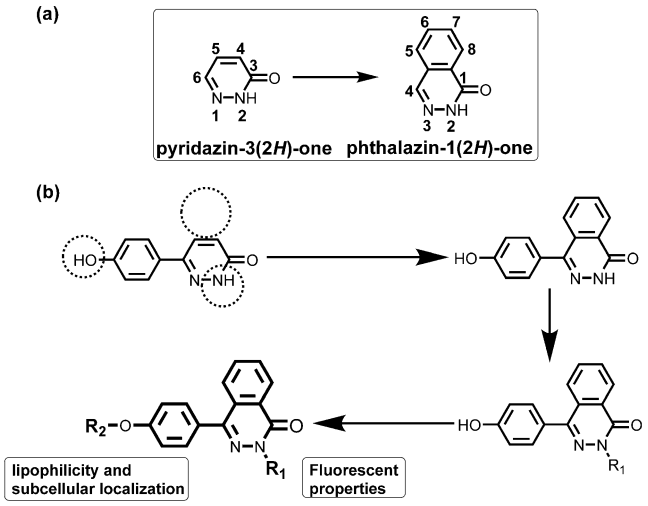

Figure 1. a) Structure of pyridazine-3(2*H*)-one and phthalazin-1(2*H*)-one. b) Design strategy of the phthalazinone derivatives as fluorescent probes based on the pyridazinone scaffold.

Then coupling with different electron-donating aromatic groups such as *N*,*N*-diethylaminophenyl, thienyl, naphthyl, and quinolyl at the 2-NH group endows the whole molecule with tunable luminescent properties (Figure 1 b). Furthermore, to achieve tailor-made specificity in intracellular localization, an anchoring group on the skeleton is necessary, so that a 4-phenoxyl group was added to the phthalazinone followed by introduction of a bromo alkyl chain at the phenolic hydroxyl group. Finally, various carriers with lipophilic and cationic properties were installed at the alkyl chain to enhance the affinity to particular organelles. For example, an *n*-butyl chain was anchored to the phenolic hydroxyl group with a terminal positively charged triphenylphosphonio group, which was expected to act as a mitochondria-directing group, and morpholino was expected to behave as a lysosome-directing group.

To gain more insight into our design of phthalazinone derivatives, calculations were performed on the thermodynamic properties and electronic transitions by geometrical optimization of their structures at the B3LYP/6-31G** level of density functional theory.[10] The vertical excitation energy from the ground state to the lowest-lying excited state in the singlet manifold was also calculated.[11]

To simplify the calculation, the modified alkyl chain linked at the phenolic hydroxyl group was omitted and replaced by a simple methyl group without influencing the results. As shown in Tables 1 and 2, as well as Table S2 of the Supporting Information, the corresponding molecules were abbreviated as **PY** for pyridazinone analogues and **PH** for phthalazinone analogues. The structurally analyzed molecular framework was composed of three aromatic rings: pyridazinone/phthalazinone, anisole, and *N*-substituent. In the optimized structures of **PY1**, **PY2**, and **PY3**, the dihedral angle between the anisole and pyridazinone rings is about 22°, but it increased to about 50° between the anisole and phthalazinone rings because of the steric effect between 2′-H of anisole and 5-H of phthalazinone. The dihedral angles between pyridazinone/phthalazinone and *N*,*N*-diethylaminophenyl rings range from 37.8 to 40°. However, this angle is only 2.6° when *N*,*N*-diethylaminophenyl is replaced by thienyl. The significant difference in dihedral angles is determined by the interaction between the carbonyl O atom and the nearest H atom of the *N*,*N*-diethylaminophenyl or thienyl group. Moreover, alkyl substitution on the amino group of aniline had no effect on the structure of the whole molecule (Supporting Information, Table S2).

For all these compounds, the $S_0 \rightarrow S_1$ transition mainly consists of HOMO→LUMO. All the aniline-containing compounds

Table 1. Calculated parameters ($S_0 \rightarrow S_1$) of different pyridazinone and phthalazinone derivatives.[a]

Compound	HOMO [eV]	LUMO [eV]	Excitation energy [eV]	f[b]	Composition	Dihedral angles[c]
PY1	−4.91	−1.61	2.88	0.3235	HOMO→LUMO	22.1/37.8
PH1	−4.84	−1.32	3.06	0.2451	HOMO→LUMO	50.2/39.6
PH6	−5.41	LUMO: −1.69 LUMO+1: −1.33	3.27	0.2493	HOMO→LUMO (94%) HOMO→LUMO+1 (6%)	48.9/2.6

[a] Only selected excited states were considered. [b] Oscillator strength. [c] The former is the dihedral angle between anisole and pyridazinone/phthalazinone moieties, and the latter is that between the *N*-substituent and the pyridazinone/phthalazinone ring.

Table 2. DFT calculated HOMOs and LUMOs of pyridazinone and phthalazinone derivatives.

Model	HOMO	LUMO
PY1	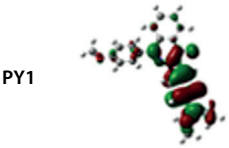	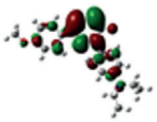
PH1	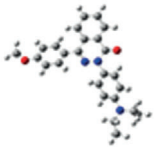	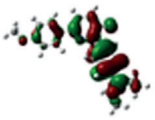
		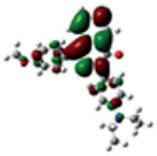
		LUMO:
		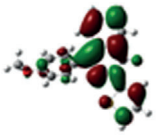
PH6	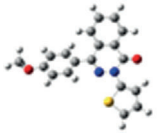	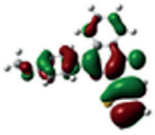
		LUMO + 1:
		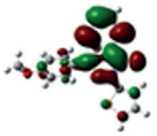

have HOMO→LUMO $S_0 \rightarrow S_1$ transitions. For compound **PH6**, 94% HOMO→LUMO and 6% HOMO→LUMO + 1 was obtained due to the thienyl group. The distribution of the molecular HOMO and LUMO reveals that $S_0 \rightarrow S_1$ transition is basically an intramolecular charge transfer from aniline to pyridazinone/phthalazinone. Alkyl substitution of the amino group enhances the HOMO energy by increasing the electron density, but it has no influence on the energy of the LUMO because the LUMO does is not located on the aniline moiety. With increasing the substituent on the amino group of the aniline moiety, the fluorescence spectrum shows a redshift and the HOMO–LUMO energy gap decreases. Compared with phthalazinone, pyridazinone showed a 25 nm redshift and increased oscillator strength due to its greater planarity. Moving the methoxyl group to the *meta* position had no effect on the planarity or electronic transition of the whole molecule (Supporting Information, Table S3). The slight spectroscopic redshift was attributed to the methoxyl group lowering the electron-donating ability of anisole, which reduces the energy of LUMO. Although **PH6** shows greater planarity, the five-membered thienyl ring reduces the repulsion between the carbonyl O atom and 5′-H of the thienyl substituent, and its weaker electron-donating ability leads to indistinct charge-transfer characteristics in a higher-energy electronic transition.

Synthesis and characterization

With the results of our calculations in hand, we started our synthesis of the phthalazinone derivatives. To prepare the target molecules, two efficient synthetic routes were explored depending on the substituents of choice.

As shown in Scheme 1, Method A was established with 2,3-dihydrophthalazine-1,4-dione (**1**) as starting material. By treatment with $POBr_3$ and acetic acid, **2** was obtained in 86% yield. Then a palladium-catalyzed Suzuki coupling reaction was used to form a C–C bond between **2** and 4-hydroxyphenylboronic acid to give **3**, which is suitable for construction of an optional substituted hydroxyl group at the 4-phenyl position of phthalazinone, in moderate to high yields. 4-(4-Hydroxyphenyl)phthalazin-1(2*H*)-one (**3**) is the core skeleton of our target compounds. Extension of **3** by coupling of an electron-donating substituent to the 2-NH group expands the conjugation and give a donor–acceptor system.[12] Moreover, modification of the hydroxyl group allows the functionality to be increased. Selective modification of **3** with different electron-donating aromatic halides by copper(I) iodide catalyzed coupling reactions proceeded with retention of the hydroxyl group. For example, after coupling with 4-bromo-*N*,*N*-diethylaniline, fluorescent product **4** was obtained in 72% yield. 2-Iodothiophene could also be used to couple with **3**, and the corresponding product was obtained in 68% yield. Then the hydroxyl group was substituted with different dibromo alkanes such as 1,4-dibromobutane and 1,6-dibromohexane in order to investigate the role of the length of the alkyl chain, which showed little effect on the structure and photophysical properties of the luminescent core. Finally, compounds **6** were obtained through terminal bromo substitution with different nucleophiles such as triphenylphosphine, morpholine, pyrrolidine, and piperidine. The total yields ranged from 18 to 32%, depending on the nucleophile. The advantage of this route lies in the 4-substituent of the phthalazinone, which could be varied by means of differ-

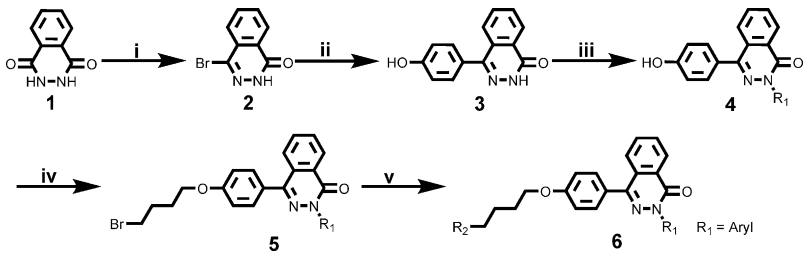

Scheme 1. Method A. Reagents and conditions: i) 1,2-Dichloroethane, $POBr_3$, reflux, 12 h; acetic acid, reflux, 2 h; ii) 4-Hydroxyphenylboronic acid, $[Pd(PPh_3)_4]$, Na_2CO_3, DMF, H_2O, 120 °C, 24 h; iii) 4-Bromo-*N*,*N*-diethylaminophenyl, CuI, Cs_2CO_3, DMF, 120 °C, 12 h; iv) 1,4-Dibromobutane, K_2CO_3, CH_3CN, reflux 4 h; v) PPh_3 or other nucleophiles, CH_3CN, reflux, 24 h.

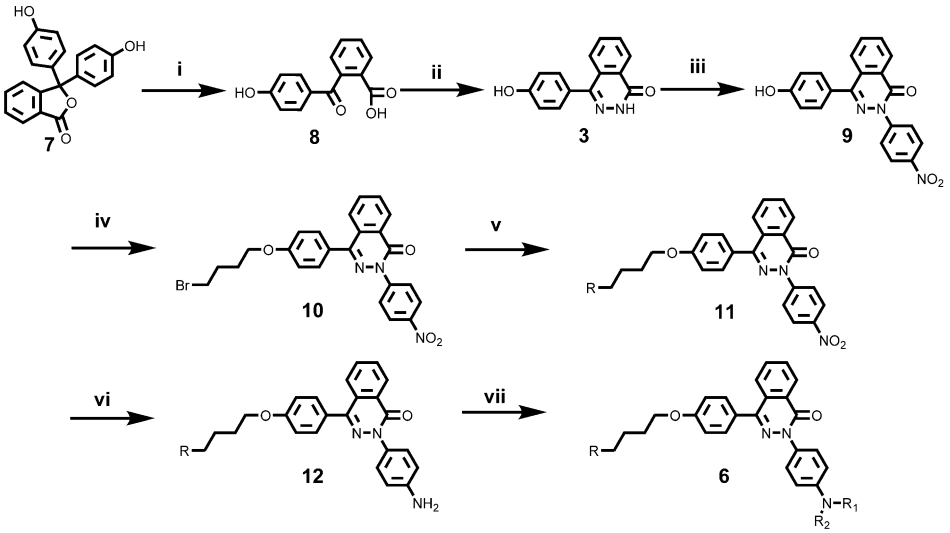

Scheme 2. Method B. Reagents and conditions: i) NaOH, hydroxylamine hydrochloride, H_2O, 80 °C; sulfuric acid, H_2O, 100 °C; ii) Hydrazine hydrate, chlorobenzene, dimethylacetamide, reflux, 2 h; iii) 1-Iodo-4-nitrobenzene, CuI, Cs_2CO_3, DMF, 120 °C, 12 h; iv) 1,4-Dibromobutane, K_2CO_3, CH_3CN, reflux, 4 h; v) PPh_3 or other nucleophiles, CH_3CN, reflux, 16 h; vi) Hydrazine hydrate, $FeCl_3{\cdot}6H_2O$, activated carbon, 1,4-dioxane, reflux 4 h; vii) Iodoethane, Cs_2CO_3, CH_3CN, reflux, 16 h.

ent aromatic boronic acids to expand the scope of our compound library.

To simplify the synthetic route with the aim of rapid synthesis of **3** with low cost and on a large scale, we explored an optimized method. As shown in Scheme 2, by treating phenolphthalein with NaOH, hydroxylamine hydrochloride, and then sulfuric acid in hot water, 2-(4-hydroxybenzoyl)benzoic acid (**8**) was obtained in quantitative yield.[13] Then the core skeleton **3** was obtained in quantitative yield by condensation of **8** with hydrazine hydrate in 2 h.[14] In another adjustment, 4-bromo-*N*,*N*-diethylaminophenyl was replaced by *p*-nitrobenzene in the copper(I) iodide catalyzed reaction at the 2-NH group of phthalazinone. To investigate the electron-donating effect of different amino groups and avoid the simultaneous substitution at both amino and hydroxyl groups, compound **9** was prepared. Its phenol group could be fully modified with retention of the nitro group. Then, we used $FeCl_3$ and hydrazine to reduce the nitro to an amino group in 94% yield.[15] The amino group could be substituted with one or two alkyl groups by a controlled procedure to give the desired products **6** in considerable total yields. The optimized route also expands the scope of our target compounds due to the variety of tailor-made substituents on the amino group. Besides, 2-iodothiophene, 2-bromonaphthalene, and 3-bromoquinoline were also employed in this route with moderate to good yields.

With the optimized synthetic route, 22 compounds were prepared in moderate to good yields. Before biological evaluation, their photophysical properties were measured. Absorption data for all the compounds are compiled in Table 3. In DMSO at 298 K, they generally show an intense band around 313–392 nm with molar absorptivity ε in the range of 0.49×10^4 to $1.68\times10^4\,M^{-1}cm^{-1}$, corresponding to the $^1\pi$–π^* transition of the basic fluorophores. To examine how the pyridazinone/phthalazinone moiety influences the photophysical properties, these two series of compounds were compared in the light of **6a** versus **6f**, **6c** versus **6g**, and **6d** versus **6o**, and the pyridazinone derivatives showed obvious redshifts. The bathochromic shift of the absorption peak may arise from the increasing electron-withdrawing ability of the pyridazinone moiety. By comparing **6f**, **6j**–**6o**, **6t**, and **6u**, all of which have the same fluorophore but different terminal modification of the alkyl chain, we found that the appended alkyl moiety has a negligible effect on the photophysical properties of these compounds (Supporting Information, Figures S1–S3).

According to our previous report, the hydrophobicity and charge of the *N*-substituents of the pyridazinone strongly affect the photophysical properties.[9] In this work, electron-donating aromatic groups such as *N*-alkylated aminophenyl, thienyl, naphthyl, and quinolyl were used for coupling with the pyridazinone and phthalazinone moiety. The results obtained for **6f**–**6i** and **6o**–**6s** indicated that the rigidity and electron-donating ability of the *N*-substituents affect the electronic structures and the absorptions of the fluorophores more significantly than variation of the pyridazinone/phthalazinone moieties.

Pyridazinone and phthalazinone derivatives with similar *N*-substituents were found to exhibit similar vibronically structured emission bands. For instance, phthalazinone **6f** with a *p*-*N*,*N*-dialkylated aminophenyl *N*-substituent showed maximum emission at 612 nm, which is blueshifted by about 24 nm compared to the similar pyridazinone analogue **6a** (636 nm).

To probe how the *N*-substituents affect the emissions of the compounds, we chose **6o**–**6s** for comparison. As shown in Table 3, they emit with a maximum at 610, 607, 497, 465, and 426 nm, respectively. Their fluorescence spectra show progressive blueshifts with decreasing electron-donating ability, as was observed in the absorption spectra.

Fluorescent quantum yields Φ_{fl} were measured in DMSO by using fluorescein as reference.[16] As shown in Table 3, the phthalazinone derivatives **6f**, **6j**–**6o**, **6t**, and **6u** have consid-

Table 3. Structures and photophysical properties of **6**.[a]

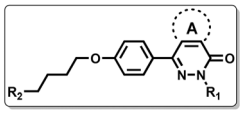

Compound	A	R_1	R_2	ε_{max}[b]	λ^1_{max}(ex)/λ^{fl}_{max}(em)[c]	Φ_{fl}[d]	λ^2_{max}(ex)
6a	1	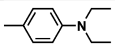	$^+PPh_3$	0.81	392/636	0.098	820
6b	1		$^+PPh_3$	0.78	380/640	0.090	820
6c	1	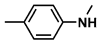	$^+PPh_3$	0.93	383/633	0.084	800
6d	1	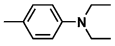		0.93	391/635	0.077	820
6e	1			0.72	382/645	0.074	820
6f	2	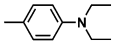	$^+PPh_3$	0.84	351/612	0.244	820
6g	2	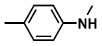	$^+PPh_3$	0.59	330/615	0.120	800
6h	2		$^+PPh_3$	1.05	355/479	0.215	800
6i	2		$^+PPh_3$	1.23	351/479	0.027	n.d.[e]
6j	2	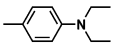	$^+P(Cy)_3$	0.60	350/613	0.213	820
6k	2	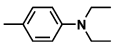	PPh_2	0.49	352/611	0.198	n.d.
6l	2	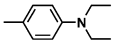		0.75	350/611	0.204	820
6m	2	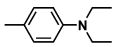		0.72	354/613	0.185	820
6n	2	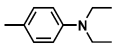	$-NEt_3^+$	0.68	351/611	0.177	820
6o	2	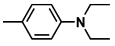		0.97	351/610	0.196	820
6p	2	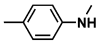		0.85	342/607	0.133	800
6q	2			1.06	353/497	0.209	800
6r	2			1.39	313/465	0.022	n.d.
6s	2			1.68	314/426	0.018	n.d.
6t	2	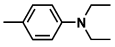		0.70	349/607	0.188	820
6u	2	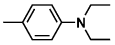		0.56	352/610	0.224	820

[a] All data were measured in DMSO at 298 K. [b] Extinction coefficient in $10^4\,M^{-1}cm^{-1}$. [c] λ_{max} values of the one-photon absorption and emission spectra in nanometers. [d] Fluorescence quantum yield, with fluorescein as standard ($\Phi = 92\%$ in 0.1 N NaOH). [e] Not determined.

erable fluorescence quantum yields (0.177–0.244), which are higher than those of pyridazinone derivatives **6a** (0.098) and **6d** (0.077). The electron-donating ability of **6a** bearing an *N*,*N*-diethylaminophenyl group exhibited higher Φ_{fl} than **6b** with an *N*,*N*-dimethylaminophenyl moiety. Singly alkylated **6c** showed lower Φ_{fl} than dialkylated analogues such as **6a** and **6b**. The same trend was also observed for phthalazinone derivatives.

Phthalazinone derivatives have never been used in two-photon fluorescence spectroscopy. To study their potential and the relationship between the 2PA cross section and the electronic structure, we measured the 2PA cross sections of compounds **6** by the two-photon induced fluorescence method referenced to fluorescein (Supporting Information, Figure S5). The compounds exhibit reasonable 2PA cross sections δ across the 740–860 nm spectral window with **6f** showing a maximum value of $\delta = 221$ GM at 820 nm.

In our previous study, the viability, stability against photobleaching, and cytotoxicity of a series of pyridazinone compounds were measured and compared with those of some commonly used fluorescent dyes such as fluorescein. Herein, commercial trackers were used for comparison to test the phthalazinone derivatives. We found that **6a** and **6f** showed obviously better properties than MitoTracker, and **6o** showed

better performance than LysoTracker (Supporting Information, Figures S6–S8). To reveal the structural relationship between the photophysical properties and the biological behaviors, the cell viabilities of the compounds were assessed by CCK-8 assay (Supporting Information, Figures S9 and S10). The results indicated that all these compounds have low cytotoxicity, even when the cell were incubated with 20 μM of the compounds for 24 h. These newly developed fluorescent dyes showed better photobleaching resistance and pH tolerance in different buffers, and thus may have potential in biological applications.

Cell imaging

Live-cell imaging experiments were performed to explore the relation between the structure of compounds **6**, their photophysical properties, and the visualization of specific cellular behaviors.

Due to the specific charge condition of the membrane of mitochondria, positively charged groups including P-/N-containing groups have been widely employed for mitochondria.[17] Herein, triphenylphosphonio was used as mitochondrion-directing group with a commercially available mitochondrial tracker as control, and excellent results were obtained. Images of SH-SY5Y cells incubated with 2 μM of **6a**, **6f**, and **6h** are shown in Figure 2. All of them exhibited high selectivity

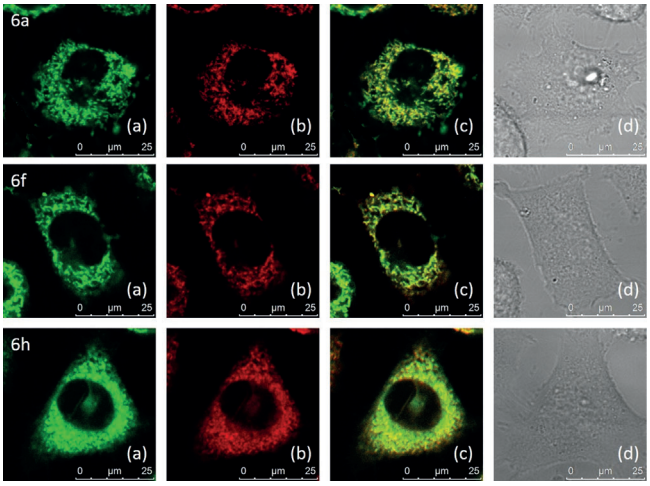

Figure 2. One-photon fluorescence colocalization images of SH-SY5Y cells incubated with 2 μM probes and commercial dyes. a) Image of **6**. b) Image of MitoTracker Deep Red FM. c) Merged images of a) and b). d) Bright-field image. Images were acquired in two channels. For channel 1 with 405 nm excitation and fluorescent emission windows: green = 450–570 nm (**6a**, **6f**), green = 420–550 nm (**6h**), and for channel 2 with 633 nm excitation and fluorescence emission windows: red = 643–700 nm.

for mitochondria, and the details are even better revealed than with MitoTracker. Their Pearson's coefficients, which are all greater than 0.90, indicate excellent colocalization with the mitochondria. Apart from aminophenyl and thienyl, neither naphthyl nor quinolyl as electron-donating group in **6i**, **6r**, or **6s** was suitable for one-photon microscopy due the poor photophysical properties. As negative control, an electroneutral diphenylphosphanyl group was used in **6k**, and poor colocalization with mitochondria was observed. For **6l**, **6m**, and **6n**, pyridinio, *N*-methylimidazolio, and triethylammonio were used as positively charged nitrogen cores in the mitochondrion-targeting component, but lower colocalization with mitochondria was verified by the confocal micrographs and Pearson's coefficients (Supporting Information, Tables S4 and S6). Compounds **6b** and **6c** based on a pyridazinone scaffold also exhibited high luminescence and colocalization, which indicated alkyl substitution on the amino group has an obvious effect on cell imaging. When triphenylphosphonio was replaced by tricyclohexylphosphonio, **6j** still showed good colocalization performance, but the distribution in the mitochondria was not even as good as that of **6f**. Besides, phthalazinone analogue **6v** with an *n*-hexyl chain showed similar features to **6f** when applied in OPM (Supporting Information, Tables S4 and S6).

With appropriate nucleophilicity and alkalinity, morpholino tails are effective in carrying the parent compounds into lysosomes.[18] The morpholino moieties of **6d**, **6e**, and **6o**–**6s** are responsible for their similar lysosomal localizations. As shown in Figure 3 and Table S5 (Supporting Information), **6d**, **6o**, and

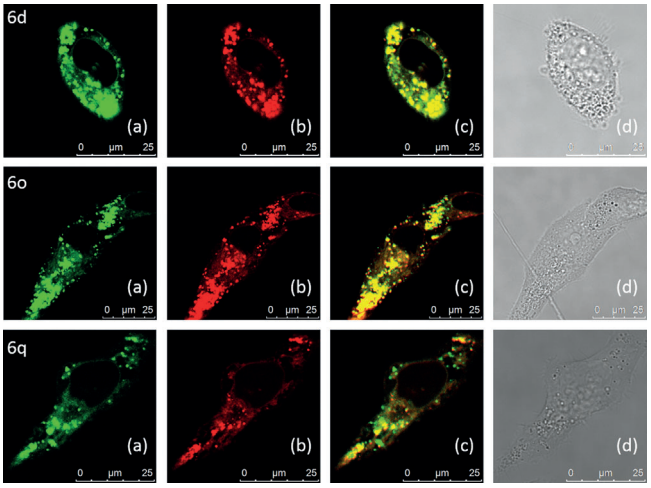

Figure 3. One-photon fluorescence colocalization images of RD cells incubated with 2 μM probes and commercial dyes. a) Image of **6**. b) image of LysoTracker Red. c) Merged images of a) and b). d) Bright-field image. Images were acquired in two channels. For channel 1 with 405 nm excitation and fluorescence emission windows: green = 420–550 nm (**6d**, **6o**), Green = 450–570 nm (**6q**), and for channel 2 with 561 nm excitation and fluorescence emission windows: red = 575–650 nm.

6q showed excellent colocalization with LysoTracker Red in both RD cells and SH-SY5Y cells. Their Pearson's coefficients are around 0.90. Since tertiary amines such as morpholine, pyrrolidine, and piperidine are widely used as leading substances for lysosomes, ,**6t** and **6u** bearing pyrrolidino and piperidino moieties, respectively, were applied, and good colocalization with commercial LysoTracker Red was observed due to the appropriate pendant groups (Figure 4).

Therefore, variation of the basic skeleton modulates the intracellular emission without disturbance of the subcellular lo-

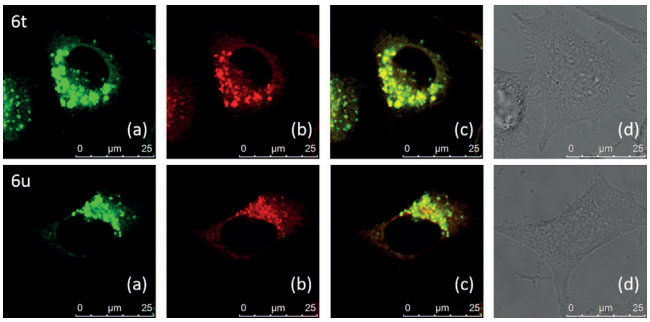

Figure 4. One-photon fluorescence colocalization images of SH-SY5Y cells incubated with 2 μM probes and commercial dyes. a) Image of **6**. b) Image of LysoTracker Red. c) Merged images of a) and b). d) Bright-field image. Images were acquired in two channels. For channel 1 with 405 nm excitation and fluorescence emission windows: green = 450–570 nm, and for channel 2 with 561 nm excitation and fluorescence emission windows: red = 575–650 nm.

calization. The terminal pendants of the alkyl chain determine the lipophilicity, with different partition coefficients, and the subcellular localizations with different affinity to specific subcellular organelles, while having negligible effect on the emission.

Two-photon imaging of brain tissue

To further establish the utility of compounds **6** for TPM bioimaging, the probes were employed to visualize mouse brain tissue. The brain slices were isolated from two-month-old mice, and each slice was incubated with 20 μM **6 f** for 30 min at 37 °C. Because the structure of the brain tissue is heterogeneous, we acquired eight TPM images at the depths of 100–200 μm to investigate the overall distribution of the fluorescence. As shown in Figure 5, **6 f** is capable of imaging in live

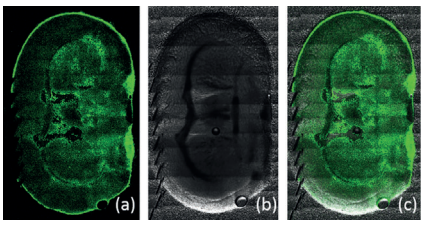

Figure 5. a) TPM image of a fresh mouse brain slice labeled with **6 f** (20 μM, 30 min). b) Bright field image. c) Merged images of a) and b). Images were acquired with 720 nm excitation and fluorescent emission windows: green = 450–570 nm.

tissue at depths ranging from 100–200 μm by TPM. Moreover, the entire brain slices, including the cerebral cortex and central core, were observed with strong fluorescence. The fluorescence intensity in the central core was not only stronger but also more stable than that in the cortex, and indicated different cell permeabilities of **6 f**.

Furthermore, **6 f** was compared with fluorescein, a commonly used fluorescent probe for brain cells. Compound **6 f** showed

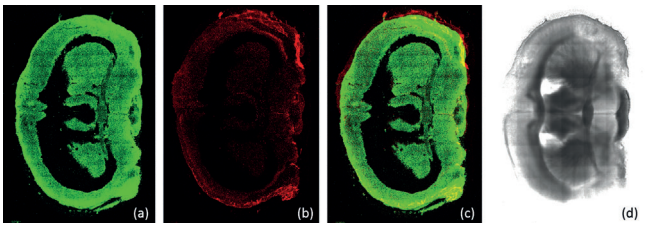

Figure 6. TPM image of a fresh rat brain slice labeled with a) **6 f** (20 μM, 30 min) and b) fluorescein (20 μM, 30 min). c) Merged image of a) and b). d) Bright-field image. Images were acquired in two channels. For channel 1 with 720 nm excitation and fluorescence emission windows: green = 450–570 nm, and for channel 2 with 488 nm excitation and fluorescence emission windows: red = 500–550 nm.

stronger luminescence and more homogeneous distribution in the brain than fluorescein (Figure 6).

Conclusion

By rational design and theoretical calculations, we constructed a pyridazinone/phthalazinone library of one- and two- photon emissive probes for use in live-cell and brain-tissue imaging. The structural relationship between the photophysical properties and the biological behaviors was elucidated. More importantly, the electronic states of the *N*-substituents of pyridazinone/phthalazinone moieties can effectively modulate the photophysical properties of the fluorescent probes, while the terminal pendants on the alkyl chain determine the lipophilicity and subcellular organelle selectivity. These novel fluorescent probes were used successfully in both one-photon cell imaging with high luminescence and subcellular organelle selectivity, and two-photon brain-tissue imaging with excellent performance exceeding those of some commercial probes, which provides an important insight into modular design of luminescent probes and further expands the repertoire of small-molecule fluorophores.

Acknowledgements

This work was supported by the National Natural Science Foundation of China (21202003/21172012/81302763/91330103), the National Basic Research Program of China (2012CB518000), and the Specialized Research Fund for the Doctoral Program of Higher Education of China (20120001110010).

Keywords: density functional calculations · fluorescence microscopy · fluorescent probes · imaging agents · synthesis design

[1] a) W. Rettig, B. Strehmel, S. Schrader, H. Seifert in *Applied Fluorescence in Chemistry, Biology, and Medicine*, Springer, New York, **1999**; b) J. J. Lavigne, E. V. Anslyn, *Angew. Chem. Int. Ed.* **2001**, *40*, 3118–3130; *Angew. Chem.* **2001**, *113*, 3212–3225; c) J. Rao, A. Dragulescu-Andrasi, H. Yao, *Curr. Opin. Biotechnol.* **2007**, *18*, 17–25; d) J. Zhang, R. E. Campbell, A. Y. Ting, R. Y. Tsien, *Nat. Rev. Mol. Cell Biol.* **2002**, *3*, 906–918.

[2] a) B. N. G. Giepmans, S. R. Adams, M. H. Ellisman, R. Y. Tsien, *Science* **2006**, *312*, 217 – 224; b) M. Vendrell, D. Zhai, J. C. Er, Y.-T. Chang, *Chem. Rev.* **2012**, *112*, 4391 – 4420; c) G. Lukinavičius, K. Umezawa, N. Olivier, A. Honigmann, G. Yang, T. Plass, V. Mueller, L. Reymond, I. R. Corrêa, Jr., Z.-G. Luo, C. Schultz, E. A. Lemke, P. Heppenstall, C. Eggeling, S. Manley, K. Johnsson, *Nat. Chem.* **2013**, *5*, 132 – 139.

[3] M. A. Paley, J. A. Prescher, *MedChemComm* **2014**, *5*, 255 – 267.

[4] a) L. M. Wysockia, L. D. Lavis, *Curr. Opin. Chem. Biol.* **2011**, *15*, 752 – 759; b) E. Kim, S. B. Park, *Chem. Asian J.* **2009**, *4*, 1646 – 1658.

[5] a) Y. Imanishi, K. H. Lodowski, Y. Koutalos, *Biochemistry* **2007**, *46*, 9674 – 9684; b) H. M. Kim, B. R. Cho, *Acc. Chem. Res.* **2009**, *42*, 863 – 872.

[6] H. M. Kim, B. R. Cho, *Chem. Rev.* **2015**, *115*, 5014 – 5055.

[7] a) A. D. Goldberg, J. Nicklas, S. Goldstein, *Am. J. Cardiol.* **1991**, *68*, 631 – 636; b) J. A. Barrett, R. H. Meacham, M. F. Kelley, Jr., W. F. Graney, M. H. Perrone, *Cardiovasc. Drug Rev.* **1990**, *8*, 323 – 338; c) R. F. Kauffman, D. W. Robertson, R. B. Franklin, G. E. Sandusky, Jr., F. Dies, J. L. McNay, J. S. Hayes, *Cardiovasc. Drug Rev.* **1990**, *8*, 303 – 322; d) R. Hudkins, R. Raddatz, M. Tao, J. Mathiasen, L. Aimone, N. Becknell, C. Prouty, L. Knutsen, M. Yazdanian, G. Moachon, M. Ator, J. Mallamo, M. Marino, E. Bacon, M. Williams, *J. Med. Chem.* **2011**, *54*, 4781 – 4792; e) D. Ukena, K. Rentz, C. Reiber, G. W. Sybrecht, *Resp. Med.* **1995**, *89*, 441 – 444; f) S. Ovais, K. Javed, S. Yaseen, R. Bashir, P. Rathore, R. Yaseen, A. D. Hameed, M. Samim, *Eur. J. Med. Chem.* **2013**, *67*, 352 – 358; g) O. Unsal Tan, K. Ozadali, P. Yogeeswari, D. Sriram, A. Balkan, *Med. Chem. Res.* **2012**, *21*, 2388 – 2394.

[8] a) J. A. Bristol, I. Sircar, W. H. Moos, D. B. Evans, R. E. Weishaar, *J. Med. Chem.* **1984**, *27*, 1099 – 1101; b) I. Sircar, B. L. Duell, G. Bobowski, J. A. Bristol, D. B. Evans, *J. Med. Chem.* **1985**, *28*, 1405 – 1413; c) S. Corsano, R. Scapicchi, G. Strappaghetti, G. Marucci, F. Paparelli, *Eur. J. Med. Chem.* **1995**, *30*, 71 – 75; d) T. Costas, P. Besada, A. Piras, L. Acevedo, M. Yañez, F. Orallo, R. Laguna, C. Terán, *Bioorg. Med. Chem. Lett.* **2010**, *20*, 6624 – 6627; e) S. Thota, R. Bansal, *Med. Chem. Res.* **2010**, *19*, 808 – 816; f) M. M. Saeed, N. A. Khalil, E. M. Ahmed, K. I. Eissa, *Arch. Pharmacal Res.* **2012**, *35*, 2077 – 2092; g) K. Özadalı, F. Özkanlı, S. Jain, P. P. N. Rao, C. A. Velázquez-Martínez, *Bioorg. Med. Chem.* **2012**, *20*, 2912 – 2922; h) Z. K. Sweeney, J. P. Dunn, Y. Li, G. Heilek, P. Dunten, T. R. Elworthy, X. Han, S. F. Harris, D. R. Hirschfeld, J. H. Hogg, W. Huber, A. C. Kaiser, D. J. Kertesz, W. Kim, T. Mirzadegan, M. G. Roepel, Y. D. Saito, T. M. P. C. Silva, S. Swallow, J. L. Tracy, A. Villasenor, H. Vora, A. S. Zhou, K. Klumpp, *Bioorg. Med. Chem. Lett.* **2008**, *18*, 4352 – 4354; i) M. Tao, L. D. Aimone, Z. Huang, J. Mathiasen, R. Raddatz, J. Lyons, R. Hudkins, *J. Med. Chem.* **2012**, *55*, 414 – 423; j) R. Raddatz, R. L. Hudkins, J. R. Mathiasen, J. A. Gruner, D. G. Flood, L. D. Aimone, S. Le, H. Schaffhauser, E. Duzic, M. Gasior, D. Bozyczko-Coyne, M. J. Marino, M. A. Ator, E. R. Bacon, J. P. Mallamo, M. Williams, *J. Pharmacol. Exp. Ther.* **2012**, *340*, 124 – 133.

[9] L. Liang, W. Wang, J. Wu, F. Xu, Y. Niu, B. Xu, P. Xu, *Chem. Eur. J.* **2013**, *19*, 13774 – 13782.

[10] a) E. Runge, E. K. U. Gross, *Phys. Rev. Lett.* **1984**, *52*, 997 – 1000; b) A. D. Becke, *J. Chem. Phys.* **1993**, *98*, 5648 – 5652; c) A. D. Laurent, D. Jacquemin, *Int. J. Quantum Chem.* **2013**, *113*, 2019 – 2039.

[11] a) J. Y. Shao, S. M. Ji, X. L. Li, J. Z. Zhao, F. Zhou, H. M. Guo, *Eur. J. Org. Chem.* **2011**, 6100 – 6109; b) Z. Chamas, E. Marchi, A. Modelli, Y. Fort, P. Ceroni, V. Mamane, *Eur. J. Org. Chem.* **2013**, 2316 – 2324.

[12] a) L. Liang, G. Yang, W. Wang, F. Xu, Y. Niu, Q. Sun, P. Xu, *Adv. Synth. Catal.* **2013**, *355*, 1284 – 1290; b) L. Liang, G. Yang, F. Xu, Y. Niu, Q. Sun, P. Xu, *Eur. J. Org. Chem.* **2013**, 6130 – 6136; c) L. Liang, W. Wang, F. Xu, Y. Niu, Q. Sun, P. Xu, *Org. Lett.* **2013**, *15*, 2770 – 2773; d) W. Wang, L. Liang, F. Xu, W. Huang, Y. Niu, Q. Sun, P. Xu, *Eur. J. Org. Chem.* **2014**, 6863 – 6867.

[13] M. H. Hubacher, *J. Am. Chem. Soc.* **1946**, *68*, 718 – 719.

[14] X. H. Zhang, S. Chen, Y. Q. Min, G. R. Qi, *Polymer* **2006**, *47*, 1785 – 1795.

[15] X. Zhang, B. Zhou, X. Sun, G. Qi, *J. Appl. Polym. Sci.* **2009**, *114*, 1397 – 1404.

[16] a) C. Xu, W. W. Webb, *J. Opt. Soc. Am. B* **1996**, *13*, 481 – 491; b) G. A. Crosby, J. N. Demas, *J. Phys. Chem.* **1971**, *75*, 991 – 1024.

[17] J. Tang, Y. Cai, J. Jing, J.-L. Zhang, *Chem. Sci.* **2015**, *6*, 2389 – 2397.

[18] a) Y. Hai, J.-J. Chen, P. Zhao, H. Lv, Y. Yu, P. Xu, J.-L. Zhang, *Chem. Commun.* **2011**, *47*, 2435 – 2437; b) D. Xie, J. Jing, Y. Cai, J. Tang, J.-J. Chen, J.-L. Zhang, *Chem. Sci.* **2014**, *5*, 2318 – 2327.

Received: March 31, 2016
Published online on ■■ ■■, 0000

FULL PAPER

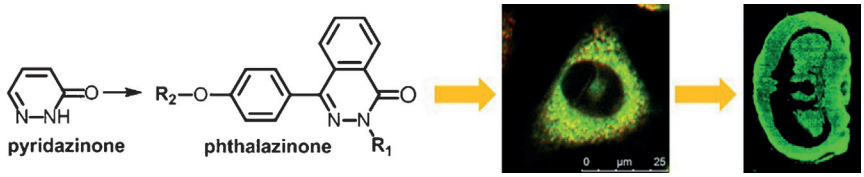

Better probes by design: A pyridazinone/phthalazinone library of one- and two-photon emissive probes for use in live-cell and brain-tissue imaging (see figure) was constructed. The electronic states of the *N*-substituents of the pyridazinone/phthalazinone moieties effectively modulate the photophysical properties of the fluorescent probes, and the terminal groups on the alkyl chain determine the lipophilicity and subcellular organelle selectivity.

Fluorescent Probes

L. Yang, Y. Zhu, M. Shui, T. Zhou, Y. Cai, W. Wang, F. Xu, Y. Niu, C. Wang, J.-L. Zhang, P. Xu, L. Yuan,* L. Liang**

■■ – ■■

Rational Design of Fluorescent Phthalazinone Derivatives for One- and Two-Photon Imaging